J. Fluid Mech. (1992), *vol.* 245, *pp.* 91–114

Viscous and inviscid instabilities of a trailing vortex

By ERNST W. MAYER AND KENNETH G. POWELL
Department of Aerospace Engineering, The University of Michigan, Ann Arbor, MI 48109, USA

(Received 8 October 1991 and in revised form 18 May 1992)

A spectral collocation and matrix eigenvalue method is used to study the linear stability of the trailing line vortex model of Batchelor. For both the inviscid and viscous stability problem, the entire unstable region in the swirl/axial wavenumber parameter space is mapped out for various azimuthal wavenumbers m. In the inviscid case, the non-axisymmetric perturbation with azimuthal wavenumber $m = 1$ has an unstable region of larger extent than any other, with an unusual two-lobed structure; also, the location and numerical value of the maximum disturbance growth rate previously reported for this case are shown to be incorrect. Exploiting the increasingly localized structure of perturbation eigenfunctions allows accurate results to be obtained up to values of m more than 3 orders of magnitude larger than previously, and the results for the most unstable mode are in excellent agreement with the asymptotic theory of Leibovich & Stewartson. A viscous analysis of these fundamentally inviscid modes reveals that the critical Reynolds number at which instability first occurs increases as $O(m^2)$ for $m \gg 1$, and finds the critical values of swirl and wavenumber, which approach limiting values as $m \to \infty$.

In the viscous case, the instabilities for $m = 0$ and 1 recently reported by Khorrami are found via a simplified numerical approach and the entire unstable region for each of these modes is mapped out over a wide range of Reynolds numbers. The critical Reynolds numbers for these modes are found to be 322.42 and 17.527, respectively, the latter having been unreported previously. The instabilities persist in the limit of large Reynolds number, with corresponding disturbance growth rates decreasing roughly as $1/Re$. In addition to the primary mode, a new family of long-wave viscous instabilities is found for the $m = 1$ case.

1. Introduction

Owing to the frequency of its occurrence and the hazard it can present to air traffic, the trailing line vortex shed by an aircraft wing has been the subject of research for a number of years. Besides being of practical interest, the study of this problem has had a number of implications for the theory of motions of swirling fluids, especially in the study of their stability. Modern theoretical work in this area goes back to the work of Howard & Gupta (1962), who considered several problems involving swirling and stratified flows and, in particular, the general problem of the linearized stability of axisymmetric swirling flow subject to three-dimensional perturbations. Howard & Gupta derived sufficient conditions for inviscid stability of, as well as a semicircle theorem for, the eigenvalues corresponding to axisymmetric perturbations of various special cases of axisymmetric steady flow; they were, however, unable to derive any general stability criteria. Barston (1980) derived a semicircle theorem in the case of non-axisymmetric perturbations, and Leibovich & Stewartson (1983) found an improved upper bound on disturbance growth rates using an energy-type integral, as

well as deriving a sufficient condition for inviscid instability of axisymmetric columnar vortices.

As none of these manipulations gives any information about the number and exact complex wave speeds of any unstable modes, however, one must resort to direct numerical calculation. Lessen, Singh & Paillet (1974) were the first to present detailed numerical calculations, finding unstable inviscid eigenmodes for the trailing vortex model of Batchelor (1964). They used a Runge–Kutta-type scheme along with the asymptotic behaviour of the solutions at large and small radial distance to integrate the disturbance equations, finding an unstable mode for swirls less than roughly $q = 1.5$ for each negative azimuthal wavenumber m, as well as an unstable mode for $m = +1$ which was stabilized at small swirl. They noted that the maximum (over q and axial wavenumber α) growth rate of the unstable mode increased monotonically with $|m|$, to $m = -6$, the limit of their calculations. Lessen & Paillet (1974) extended the inviscid analysis to include the effects of viscosity on the stability of the inviscid modes, finding low critical Reynolds numbers for the first few of these. Leibovich & Stewartson (1983) investigated this class of unstable modes for negative azimuthal wavenumbers m and showed that the maximum growth rate asymptotes to an upper limit as $|m| \to \infty$. They also developed a large-azimuthal-wavenumber asymptotic theory to obtain accurate estimates of the most unstable eigenvalue for values of $|m|$ of 3 and greater. They found that when the most unstable mode is close to neutral stability, a number of eigenmodes become asymptotically close. Later work by these authors (Stewartson & Leibovich 1987; Stewartson & Capell 1985) uses asymptotics to untangle these near-neutral modes. Duck (Duck & Foster 1980; Duck 1986) was the first to compare calculated maximum growth rates for m larger than $O(1)$ with the large-m asymptotics, going up to $m = 15$.

More recently, Khorrami (1991) has reported viscous instabilities for azimuthal wavenumbers of $m = 0$ and 1 for the trailing vortex, providing the first direct evidence that viscosity can have a destabilizing effect on swirling flow. These instabilities are of great interest both physically, since their growth rates and physical characteristics compare more favourably with instabilities observed in aircraft contrails than do the inviscid modes; and mathematically, since the axisymmetric mode exhibits the novel phenomenon of an unstable mode which does not possess a critical layer.

The motivations for the present study are as follows: previous studies of the inviscid stability of the trailing vortex have not mapped out more than a small part of the unstable region for any azimuthal wavenumber, so a detailed 'topography of instability' is of considerable interest. The second goal is to provide a numerical validation of the large-azimuthal-wavenumber asymptotics of Leibovich & Stewartson for the most unstable inviscid mode, since previous studies provide numerical results only up to $|m| = 15$. Additionally, an analysis of the effect of viscosity on the inviscid modes, particularly at larger azimuthal wavenumbers, is needed. Finally, a study of the topography of the viscous modes found by Khorrami, particularly at larger Reynolds numbers, is desirable, as are the critical parameters for the asymmetric viscous mode, which were not reported by the latter author.

2. Inviscid analysis

2.1. *The steady flow*

The steady flow is the similarity solution of Batchelor (1964) for a viscous axisymmetric line vortex far downstream from the leading edge where it is shed.

Cylindrical polar coordinates $(\tilde{r}, \theta, z)$ are used, with the z-axis coinciding with the vortex axis. In non-dimensional form this similarity solution has radial, azimuthal and axial velocity components of the form

$$U(r) = 0, \quad V(r) = (q/r)(1-\mathrm{e}^{-r^2}), \quad W(r) = W_\infty + \mathrm{e}^{-r^2}, \tag{1}$$

where $r \propto \tilde{r}/z^{\frac{1}{2}}$ is the similarity variable and the parameter q characterizes the swirl intensity of the vortex. As a consequence of Galilean invariance, the constant scaling in the axial velocity can be arbitrarily chosen without affecting the stability results. In this study W_∞ is taken to be zero, so that the real part of any eigenvalue found will give the disturbance velocity relative to the uniform axial velocity of the outer flow.

2.2. *Governing equations*

When infinitesimal disturbances of the form

$$(\tilde{u}, \tilde{v}, \tilde{w}, \tilde{p}) = [\mathrm{i}u(r), v(r), w(r), p(r)] \exp\{\mathrm{i}[\alpha(z-ct)+m\theta]\} \tag{2}$$

(where α is the axial wavenumber, c is the disturbance phase speed and m is the azimuthal wavenumber) are superimposed on the steady solution and the result substituted into the full, time-dependent, non-dimensional inviscid equations of motion, the following set of linear ordinary differential disturbance equations results:

$$u^* + mv/r + \alpha w = 0, \quad \gamma u + 2Vv/r - p' = 0, \tag{3a, b}$$

$$\gamma v + V^* u + mp/r = 0, \quad \gamma w + W' u + \alpha p = 0, \tag{3c, d}$$

where $\gamma = mV/r + \alpha(W-c)$, $(\,)^* = (\,)' + (\,)/r$ and primes denote differentiation with respect to r. Note that in the case of steady flow with non-negligible radial velocity, there are additional terms which appear in the three disturbance momentum equations; these are included in the full viscous equations, which can be found in §3.1. The boundary conditions as originally derived by Batchelor & Gill (1962) are

$$r = 0: \begin{cases} u = v = 0, \quad w \quad \text{and} \quad p \quad \text{finite if} \quad m = 0, \\ u' = u + mv = w = p = 0 \quad \text{if} \quad |m| = 1, \\ u = v = w = p = 0 \quad \text{if} \quad |m| > 1, \end{cases} \qquad r \to \infty: \quad u, v, w, p \to 0. \tag{3e}$$

Substituting a Taylor expansion about $r = 0$ of the radial and swirl disturbance velocities in (3a) shows that for $|m| = 1$, the inner boundary conditions on u and v can be replaced with

$$u'(0) = v'(0) = 0. \tag{3f}$$

The symmetries of the stability problem have been examined by several authors (Lessen *et al.* 1974; Khorrami 1991); we only note that instead of looking at both positive and negative azimuthal wavenumbers m and non-negative swirl, we will consider non-negative m and let the swirl parameter q vary along the entire real line; both approaches are equivalent in that they cover the entire parameter space.

For the analysis of temporal stability, α is taken to be real and non-negative whereas c is complex. The above system then constitutes an eigenvalue problem for the eigenvalue $\omega = \alpha c$, with the sign of the imaginary part of the eigenvalue determining whether the given disturbance is stable or not. If ω has positive imaginary part, the flow is unstable and the disturbance grows exponentially with

time. In the inviscid case, each unstable mode has a complex-conjugate counterpart, travelling with the same real wave speed, which is exponentially damped. The above system can be reduced to the following second-order equation in the radial perturbation:

$$\gamma^2(su^*)' - \left\{\gamma^2 + \gamma r\left[\frac{s}{r}\left(\gamma' + \frac{2mV}{r^2}\right)\right]' + \frac{2\alpha s V}{r^2}(mW' - \alpha r V^*)\right\} u = 0, \tag{4}$$

where $s = r^2/(m^2 + \alpha^2 r^2)$. This reduction was first performed by Howard & Gupta (1962) and is the starting point for most analytical work on this problem.

2.3. *Numerical approach*

A spectral collocation method with Chebyshev polynomial basis function (Boyd 1989; Gottlieb & Orszag 1977) is used for all the calculations in this study. To maximize the efficiency of the method it is desirable to reduce the governing equations to the smallest set of equations which contain the eigenvalue term γ linearly. The Howard–Gupta reduction (4) has thus gone too far, and a different formulation is necessary. By eliminating the pressure term between (3*b*, *d*) and (3*c*, *d*), then using (3*a*) to eliminate the axial velocity perturbation from the result, the following set of equations in the radial and azimuthal perturbations is obtained:

$$\gamma\left[\alpha u - \frac{1}{\alpha}\left(u^* + \frac{mv}{r}\right)'\right] - \frac{\gamma'}{\alpha}\left(u^* + \frac{mv}{r}\right) + (W'u)' + \frac{2\alpha V v}{r} = 0, \tag{5a}$$

$$\gamma\left[\alpha r v + \frac{m}{\alpha}\left(u^* + \frac{mv}{r}\right)\right] + (V^* - mW')\,u = 0. \tag{5b}$$

This third-order system contains the eigenvalue linearly, as desired. The inner boundary conditions (3*e*, *f*) on u and v are enforced; the requirement that perturbations decay to zero at infinity is approximated by setting $u = 0$ at a finite outer-boundary radius R. The above equations are discretized on the interval $[0, R]$, which is mapped algebraically to $[-1, 1]$, with values of the basis functions and their derivatives at the collocation points calculated using the standard three-term recurrence relation for Chebyshev polynomials. The resulting matrix eigenvalue problem of the form $\boldsymbol{A}\boldsymbol{x} = \lambda \boldsymbol{B}\boldsymbol{x}$ is first reduced to standard form using an algorithm similar to that described by Gary & Helgason (1970); the eigenvalues are then found using a complex QR algorithm (Wilkinson 1965; Golub & VanLoan 1989).

In the calculations, both the numerical outer-boundary radius R and number of basis functions per independent variable N were increased with each iteration until convergence of the eigenvalues to within a specific error bound was achieved. An example is the highly unstable case $m = 1, q = -0.5, \alpha = 0.5$. Using 64-bit arithmetic and N up to 200, the best approximation to the most unstable eigenvalue (which will also be referred to as the 'primary mode') is

$$\omega_1 = 0.049\,718\,649\,917\,4 + 0.202\,628\,101\,294\,2\mathrm{i},$$

all figures being significant. The eigenvalues corresponding to the second and third modes for this case are

$$\omega_2 = -0.016\,208\,888\,89 + 0.105\,823\,189\,54\mathrm{i}, \quad \omega_3 = -0.029\,538\,003 + 0.060\,053\,650\mathrm{i}.$$

Note that for these results the accuracy deteriorates as the eigenmode becomes more stabilized. This property appears to be a result of two effects. The first is due to the

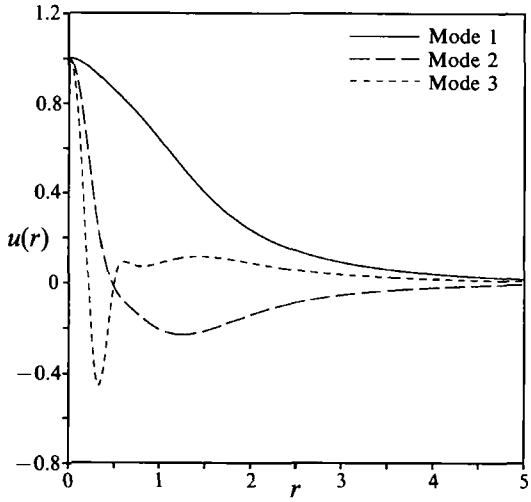

FIGURE 1. Radial velocity perturbation eigenfunctions for the three most unstable modes for the case $m = 1$, $q = -0.5$, $\alpha = 0.5$.

spurious eigenvalues arising from the discretization of the problem and affects only the convergence of inviscid eigenmodes. The spurious eigenvalues due to the discretization (which will be referred to as 'discretization modes') tend to arrange themselves in patterns in the complex plane which resemble discrete points along closed curves symmetric about the real axis. Our numerical experiments reveal that an eigenvalue of the inviscid stability problem (when there are unstable modes present) will only converge if it lies outside this discretization spectrum. The general effect of increasing the number of basis functions is to squeeze the discretization spectrum closer to the real axis, hence the closer to neutral an eigenvalue is, the higher the resolution needed to reveal it.

The second effect has to do with the actual structure of the eigenfunction for the given mode. Examination of the eigenfunctions reveals that the more unstable an eigenmode, the simpler its structure (using any reasonable criterion such as the number of zeros or inflexion points) hence the lower the number of basis functions needed to resolve it. The eigenfunctions corresponding to the radial velocity perturbation for the above three unstable modes are plotted in figure 1 to illustrate this behaviour – the number of zeros (at finite r) of the first, second and third modes is 0, 1 and 2, respectively; the number of inflexion points is 1, 3 and 5. This early convergence of unstable modes makes it relatively easy to ascertain that the most unstable mode has been found for a particular case, something which is difficult to do using local iterative methods, since the initial guess becomes all-important with the latter.

The calculations are quite straightforward and the convergence good when the mode in question is not near the neutral condition. When a mode is close to neutral stability, the singularities in the inviscid equations associated with the presence of critical layers (points where $\gamma = 0$) move close to the real axis and convergence of the eigenvalue via any numerical approach deteriorates unless extra steps are taken. In the case of shooting methods the contour of integration is deformed around the singularities associated with the desired eigenmode, a procedure described in some detail by Lin (1966). When using a global method one is not integrating the equations per se, but the deformation technique can still be used to good effect (cf. Boyd 1989).

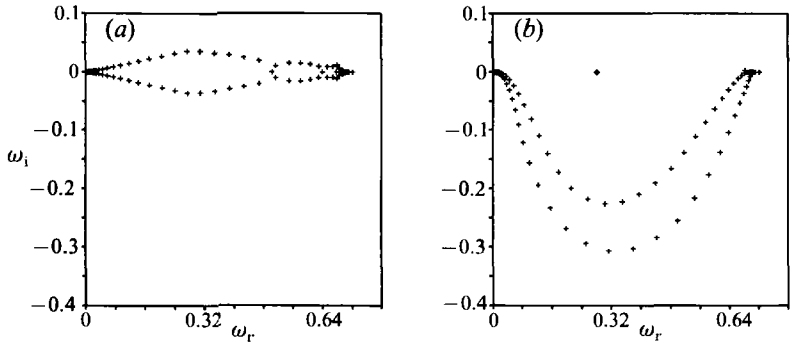

FIGURE 2. Effect of contour deformation on the discretization spectrum (open symbols) around a marginally stabilized mode (closed symbol); $m = 1$, $q = 0.074$, $\alpha = 0.63$, $R = 10$ for both cases. (*a*) $\delta = 0$, (*b*) $\delta = 1$.

Since a global matrix method must in effect deal with the singularities associated with many modes, contour deformation is not as sharp a tool as it is when integrating to find a single mode; nevertheless it is the only way to find near-neutral or marginally stabilized modes.

The contour used by Leibovich & Stewartson (1983) is the following deformation of the real variable r:

$$\hat{r} = r[1 - \mathrm{i}\delta(1 - r/R)\gamma'(r)], \tag{6}$$

where the prime denotes differentiation with respect to r. The values of the basis functions and their derivatives at the complex collocation points along this contour are evaluated using a complex three-term recurrence relation, and the coefficients due to the steady velocities are obtained from the corresponding complexification of the velocities in (1). Figure 2(*a*, *b*) demonstrates the effect of contour deformation on the spectrum of the case $m = 1$, $q = 0.074$, $\alpha = 0.63$, which lies just outside the neutral stability curve for the primary mode. Without any deformation, the eigenvalue corresponding to the primary mode is inaccessible no matter how many basis functions are used. Figure 2(*a*) shows the spectrum for $\delta = 0$, with $R = 10$ and 120 basis functions per variable. Figure 2(*b*), the same case but with $\delta = 1$, shows that deforming the contour shifts most of the discretization spectrum below the real axis, revealing the marginally stabilized mode, which has eigenvalue $\omega = 0.2822 - 0.00008\mathrm{i}$. It should also be noted that as the most unstable mode passes through the neutral point and becomes strictly stable, deformation of the contour becomes the only way to resolve it directly, but good data for marginally unstable cases often allow the neutral curve to be accurately extrapolated instead. Deforming the contour is also important in calculations where there are multiple unstable modes, since it allows the more stabilized of these to be revealed with a lower number of basis functions than would otherwise be necessary.

2.4. *Topography of the inviscid instabilities*

For azimuthal wavenumbers where an instability was found, the (q, α)-plane was discretized and the stability equations solved numerically at each point. No unstable modes were found for the case of axisymmetric disturbances $m = 0$. Of all the non-axisymmetric disturbances, the case of $m = 1$ was found to have the largest unstable region. This also is the only case where the unstable region crosses the axis of zero swirl. Contours of disturbance growth rate for this case are pictured in figure 3, with

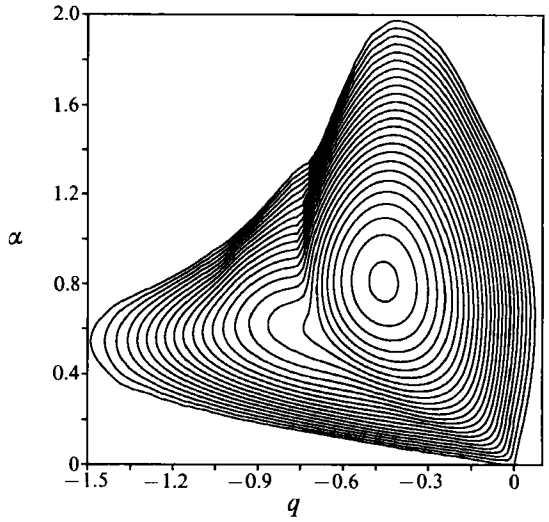

FIGURE 3. Most unstable mode for $m = 1$: contours of constant disturbance growth rate (outermost contour is neutral curve; spacing between contours is 0.01).

each contour representing an increment of 0.01 and the outermost contour being the neutral stability curve. Lessen *et al.* (1974) cite the stabilization at small positive values of swirl of this mode, their numerical results showing the imaginary part of the complex wave speed passing smoothly through zero as the swirl becomes stronger. Our results indicate stabilization of this mode at a maximum swirl of $q = +0.0739$ and a wavenumber of $\alpha = 0.63$, critical values which are in good agreement with those found by the above authors. As q is reduced from this value, the range of unstable wavenumbers increases rapidly, with the non-swirling flow unstable for $0 < \alpha < 1.18$. The unstable region has a much larger extent in the negative-swirl quarter plane, and this is also where the maximum disturbance growth rate occurs. For q decreasing from zero, long-wave disturbances are again stabilized, but the neutral curve continues to extend to shorter and shorter wavelengths. The shortest unstable wavelengths occur at $q \approx -0.42$, where the unstable region extends very nearly to $\alpha = 2$. Lessen *et al.* found a maximum growth rate of $\omega_i = 0.147$ for this mode at $q = -0.32$, $\alpha = 0.30$, which is in good agreement with the present results at those parameter values ($\omega_i = 0.1494$), but it is clear from the figure that this is well away from the actual maximum of $\omega_i = 0.2424$, which occurs at $q = -0.458$, $\alpha = 0.811$. It is likely that the numerical approach of Lessen *et al.* failed to find the most unstable mode for parameter values near these, an error which, given their use of a local method, would only have become obvious had the instability been mapped out in detail, as it is here.

Also evident from figure 3 is that at the origin the two branches of the neutral curve intersect to form a cusp, the upper branch extending to the maximum axial wavenumber mentioned above and the lower branch to the most negative value of swirl for which instability exists of $q \approx -1.5$. The general shape of the unstable region is quite interesting – the level curves of disturbance growth rate form a two-lobed structure, with a prominent ridge separating the lobes, which intersects the neutral curve at roughly $q = -0.7$, $\alpha = 1.3$ and gradually weakens and disappears in the interior of the unstable region. While derivatives of the complex wave speed might appear from this figure to be discontinuous across this ridge, an examination

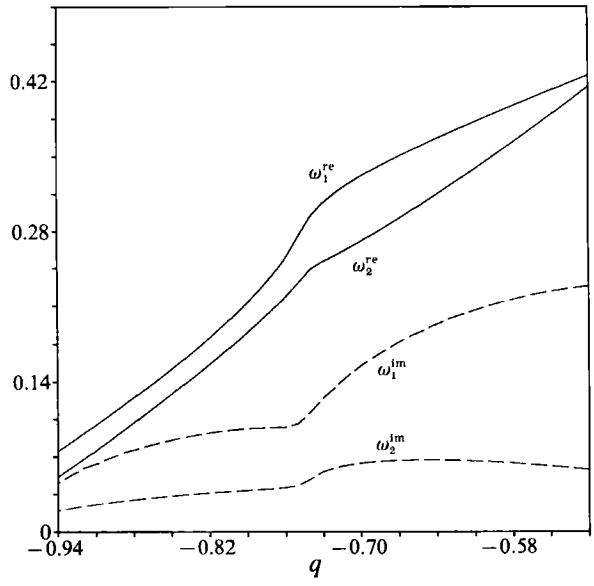

FIGURE 4. Behaviour of the two most-unstable eigenvalues across the 'ridge' at fixed $\alpha = 1$.

of the local behaviour, illustrated in figure 4 (showing real and imaginary parts of the eigenvalues corresponding to both the primary and secondary mode), reveals that eigenvalues vary smoothly there, although their first- and higher-order derivatives (with respect to q and α) vary quite rapidly. The real wave speed of the most-unstable mode varies from $\omega_r \approx 1.5$ at the upper neutral point to $\omega_r \approx -1$ at the lower, and the contour of zero phase speed exactly intersects the origin, so the longest unstable waves travel at the same speed as the outer flow.

For this azimuthal wavenumber, as many as ten unstable modes were found simultaneously in some regions of the parameter space by the numerical method. The neutral curves for the unstable modes form a nested set, with the size of the unstable region decreasing monotonically with increasing stabilization of the corresponding mode. There are two points where the neutral curves of several (perhaps all) unstable modes become asymptotically close – the lower neutral point at $q \approx -1.5$, $\alpha \approx 0.54$ and the origin. The closeness of modes near the lower neutral point was postulated for large m in Leibovich & Stewartson (1983), and was investigated in detail in Stewartson & Leibovich (1987), but its occurrence at low values of m was not reported. These authors also mention a clustering of neutral curves near the upper neutral point, but the present study is unable to confirm this for low azimuthal wavenumbers by direct calculation, as the numerical quality of solutions degrades rapidly in this region of the parameter space.

Contours of the growth rate for the second, third and fourth modes are presented in figure 5(*a–c*). The ridge seen for the primary mode is also apparent here, actually leading to a local maximum in the growth rate, distinct from the global maximum, for the second mode. The location of the maximum growth rate shifts to a more negative swirl and lower axial wavenumber for each higher mode, behaviour summarized in table 1 for the five most unstable modes, the asterisks denoting the parameter values corresponding to the maximum instability.

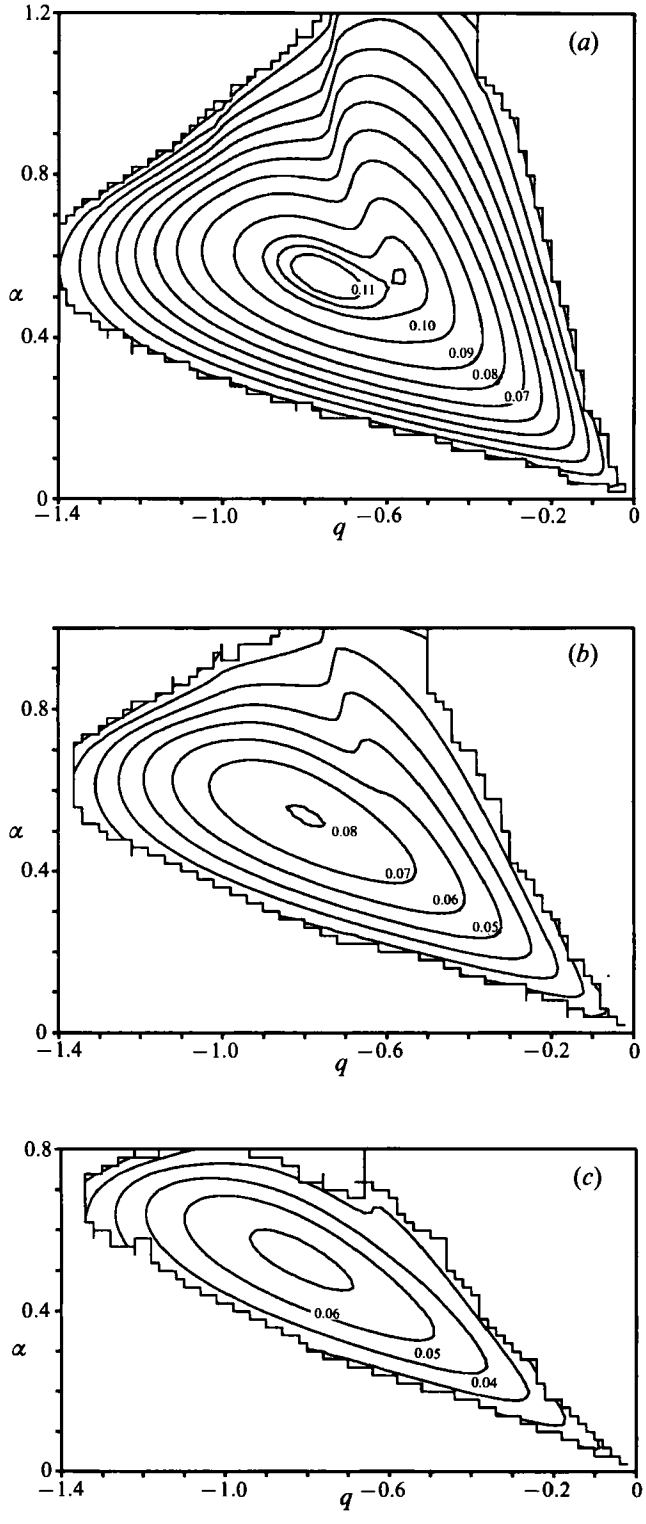

FIGURE 5. Contours of constant growth rate for higher modes in the case $m = 1$: (*a*) second mode, (*b*) third mode, (*c*) fourth mode.

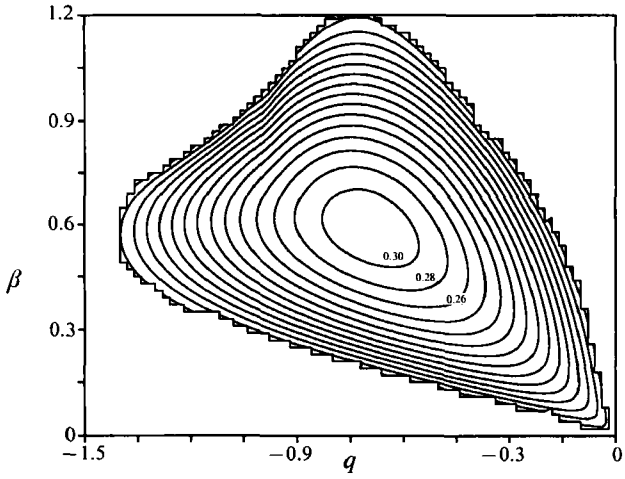

FIGURE 6. Most unstable mode for $m = 2$: contours of constant growth rate.

Mode number j	q_j^*	α_j^*	ω_j^{im}
1	−0.46	0.81	0.2424
2	−0.75	0.55	0.1116
3	−0.80	0.54	0.08046
4	−0.82	0.53	0.06222
5	−0.83	0.53	0.05030

TABLE 1. Location of maximum growth rate versus the mode number for the case $m = 1$

2.5. *The structure of instability at higher azimuthal wavenumbers*

Contour plots of the imaginary part of the eigenvalue for the most unstable mode for the case $m = 2$ are presented in figure 6, with the ordinate in the plot being the scaled axial wavenumber $\beta = \alpha/m$. The maximum growth rate for this mode of 0.3138 occurs at $q = -0.693$, $\alpha = 0.591$. The unstable region is not as large (relative to the scaled parameter space) as that for the $m = 1$ case cited in the previous section – the maximum swirl for which instability occurs is slightly greater than -1.5 and the maximum unstable wavenumber β is a bit greater than 1.2. The unstable region again has a two-lobed structure, but it is much less pronounced than for the $m = 1$ case, and shows no local ridges, appearing to be everywhere quite smooth. The modal structure is nested as before, with the locations for the maximum growth rates showing the same trend of moving to more negative swirl and lower α with increasing mode number. The real wave speeds for all cases with $m > 1$ are normalized with the azimuthal wavenumber as $\tilde{\omega}_{\mathrm{r}} = \omega_{\mathrm{r}}/m$; for $m = 2$, $\tilde{\omega}$ varies roughly between 0.5 at the upper neutral point and -0.8 at the lower, and the contour of zero phase speed again intersects the origin, as in the $m = 1$ case.

The unstable regions for $m \geqslant 3$ are qualitatively quite similar to the $m = 2$ case and are not plotted; the interior angle of the neutral curve cusp for the most unstable mode decreases, albeit slowly, with increasing m and appears to approach a finite value as $m \to \infty$. As reported in the analyses of Stewartson & Capell (1985) and Stewartson & Leibovich (1987), the maximum swirl and wavenumber for which instability occurs also asymptote to finite values in this limit, and their results, being

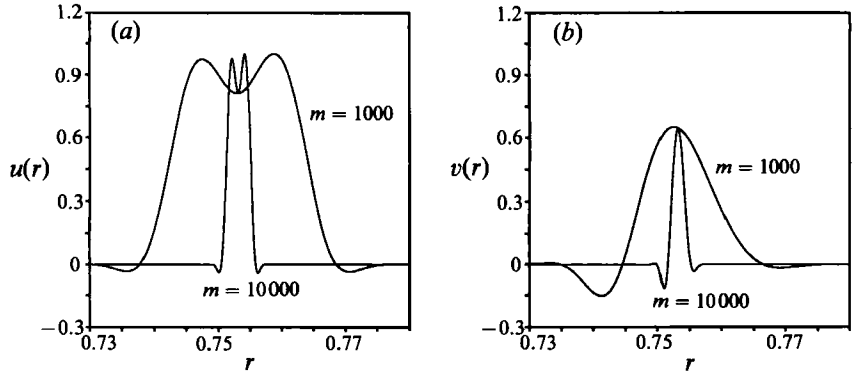

FIGURE 7. Localization of the eigenfunctions for $m \gg 1$: (*a*) radial velocity perturbation, (*b*) azimuthal velocity perturbation.

specialized to near-neutral conditions, are a more reliable guide to the extent of the unstable region in the parameter space. These facts, taken together, indicate that the entire nested modal structure becomes asymptotically close in this limit, forming a sort of 'onion skin' structure.

The analysis of the above authors also provides a clue as to why straightforward numerical calculation becomes difficult for large m. They observed that the eigenfunctions of the problem become quite localized with increasing azimuthal wavenumber, being essentially zero except in a small range of the radial variable, which led them to call these solutions 'ring modes'. For $m \gg 1$, this localization, along with the behaviour of solutions near the origin, become the key factors limiting the convergence of the standard numerical scheme. Since $u \sim r^{m-1}$ for small r, the eigenfunction requires a basis set with $O(m)$ elements to approximate this behaviour. Using a lower-order approximation leads to oscillations in the numerical approximation to the eigenfunction near the origin which contaminate the eigenvalues if their amplitude becomes sufficiently large. However, since the eigenfunction is essentially zero in a neighbourhood of the origin, it is unnecessary to approximate it there. Moving the numerical boundaries close to the critical layer to bracket the support of the unstable eigenfunctions (defined here as the interval where the amplitude of an eigenfunction is greater than some small fraction of its maximum value) provides a simple way of improving the accuracy of the calculation. The local interval is again mapped to $[-1, 1]$ and the equations discretized as before, the boundary conditions being to set u and v to zero at the endpoints. With a proper choice of the inner and outer numerical boundary (this can be guided by eigenfunction plots for lower m at the same q and α), exceptionally good results can be obtained – six-figure accuracy or better with 30 basis functions per variable is not unusual, and the accuracy shows little deterioration for a large range of m.

The localizing of the eigenfunctions about the single critical layer associated with each mode is illustrated in figure 7(*a*, *b*), where the radial and azimuthal eigenfunctions of the most unstable modes for $m = 1000$ and $m = 10000$ are plotted. It is apparent that, except for a narrowing about the critical layer, the shape of the eigenfunctions does not change significantly with increasing m. This effect can be quantified by measuring the radial spacing between two distinguished points on the eigenfunctions (the two minima which occur just inside the decaying 'tails' of the radial eigenfunction work quite nicely) for various values of m – our numerical results indicate with a high degree of accuracy that this narrowing goes as $m^{-\frac{3}{4}}$, which is in complete agreement with the asymptotic results. The growth rates of multiple

unstable modes coincide to $O(m^{-\frac{1}{2}})$ for large m; the real wave speeds (having been scaled with m^{-1}) coincide to $O(m^{-\frac{3}{2}})$.

The results for the most unstable modes are summarized in tables 2 and 3. Table 2 compares the numerical results of Lessen *et al.* for $1 \leqslant m \leqslant 6$, the asymptotic results of Leibovich & Stewartson and the numerical results of the present study for azimuthal wavenumbers up to $m = 40000$. The excellent agreement between the present numerical results and the asymptotics is apparent, as is the approach to limiting values of both location and value of the maximum disturbance growth rate, which asymptotes to 0.45876, the value at infinity being extrapolated from the $m = 20000$ and $m = 40000$ cases.

Table 3 presents data (at the same values of q^* and α^* as given in table 2) on the spatial localization of the eigenfunctions with increasing m, as well as the increasing closeness of unstable modes, illustrated with the primary and secondary mode. The approach of the maximum growth rate of the most-unstable mode to its limiting value is also presented, the difference between the value at finite m and the limiting value, $\omega_1^{\mathrm{im}}(\infty)$, vanishing as $m^{-\frac{1}{2}}$. The scaled real wave speed $\tilde{\omega}_1^{\mathrm{re}}$ asymptotes to a value of roughly -0.363614.

3. Viscous analysis

Until quite recently, the effect of viscosity on swirling flows such as the one considered here had been believed to be a purely stabilizing one. Lessen & Paillet (1974), in their second paper on the subject, considered the full viscous linearized stability equations. They found that all the inviscid instabilities described in the previous section were stabilized with increasing viscosity, with the $m = 1$ case having a critical Reynolds number of only 13.9. No viscous instability was found by them. More recently, Khorrami (1991), using a spectral collocation method and outer-boundary radii much larger than those used by Lessen & Paillet, found viscous instabilities for the azimuthal wavenumbers $m = 0$ and 1 for a wide range of Reynolds numbers, with disturbance growth rates that were typically orders of magnitude smaller than those of unstable inviscid disturbances. These instabilities occur in regions of the parameter space where no inviscid instabilities have been found, and are particularly significant because they are in good qualitative agreement with disturbances observed in experimental studies of aircraft contrails at high altitudes. As with the inviscid problem, it is desirable to map out the entire unstable region for these viscous instabilities at various values of the Reynolds number, and to study their behaviour in the limit of vanishing viscosity.

3.1. *Governing equations and numerical procedure*

The full equations governing the viscous stability to small perturbations of an axisymmetric steady flow are, using the notation of the previous section,

$$u^* + mv/r + \alpha\omega = 0, \tag{7a}$$

$$\frac{\mathrm{i}}{Re}(u')^* - \mathrm{i}(Uu)' + \left[\gamma - \frac{\mathrm{i}}{Re}\left(\frac{m^2+1}{r^2} + \alpha^2\right)\right]u + \frac{2}{r}\left(V - \frac{\mathrm{i}m}{rRe}\right)v - p' = 0, \tag{7b}$$

$$\frac{\mathrm{i}}{Re}(v')^* - \mathrm{i}Uv^* + \left[\gamma - \frac{\mathrm{i}}{Re}\left(\frac{m^2+1}{r^2} + \alpha^2\right)\right]v + \left(V^* - \frac{2\mathrm{i}m}{r^2 Re}\right)u + \frac{mp}{r} = 0, \tag{7c}$$

$$\frac{\mathrm{i}}{Re}(w')^* - \mathrm{i}Uw' + \left[\gamma - \frac{\mathrm{i}}{Re}\left(\frac{m^2}{r^2} + \alpha^2\right)\right]w + W'u + \alpha p = 0, \tag{7d}$$

	Lessen *et al.*			Leibovich & Stewartson			Present study		
m	q^*	β^*	ω^{im}	q^*	β^*	ω^{im}	q^*	β^*	ω^{im}
1	−0.32	0.3	0.1470	—	—	—	−0.458	0.811	0.24244
2	−0.70	0.6	0.3138	—	—	—	−0.693	0.591	0.31382
3	−0.79	0.57	0.3544	−0.845	0.536	0.346	−0.779	0.555	0.35459
4	−0.82	0.54	0.3777	−0.856	0.532	0.373	−0.815	0.544	0.37773
5	−0.83	0.52	0.3912	−0.865	0.531	0.390	−0.833	0.539	0.39217
6	−0.83	0.53	0.4008	−0.862	0.531	0.400	−0.844	0.536	0.40193
10	—	—	—	—	—	—	−0.861	0.531	0.42152
20	—	—	—	—	—	—	−0.870	0.529	0.43627
50	—	—	—	—	—	—	−0.872	0.529	0.44599
100	—	—	—	—	—	—	−0.872	0.530	0.45006
1000	—	—	—	—	—	—	−0.871	0.531	0.45610
10000	—	—	—	—	—	—	−0.871	0.531	0.45792
40000	—	—	—	—	—	—	−0.871	0.531	0.45834
∞	—	—	—	−0.870	0.532	0.459	−0.871	0.531	0.45876

TABLE 2. Comparison of location and value of the maximum growth rate for various azimuthal wavenumbers between the numerical results of Lessen *et al.*, the asymptotic theory of Leibovich & Stewartson, and the numerical results of the present authors

	$m = 10$	$m = 100$	$m = 1000$
R_1	NA	0.64890	0.73588
R_2	NA	0.84865	0.77050
$(R_2 - R_1)m^{\frac{3}{4}}$	NA	6.317	6.156
ω_1^{im}	0.42152	0.45006	0.456099
ω_2^{im}	0.36299	0.43301	0.450782
$(\omega_1^{\mathrm{im}} - \omega_2^{\mathrm{im}})m^{\frac{1}{4}}$	0.1851	0.1705	0.1681
$\tilde{\omega}_1^{\mathrm{re}}$	−0.349775	−0.3648211	−0.36361089
$\tilde{\omega}_2^{\mathrm{re}}$	−0.347894	−0.3646759	−0.36360575
$(\tilde{\omega}_1^{\mathrm{re}} - \tilde{\omega}_2^{\mathrm{re}})m^{\frac{3}{4}}$	0.0598	0.1452	0.1622
$\lvert\omega_1^{\mathrm{im}} - \omega_1^{\mathrm{im}}(\infty)\rvert m^{\frac{1}{4}}$	0.1178	0.0870	0.0841
$\lvert\tilde{\omega}_1^{\mathrm{re}} - \tilde{\omega}_1^{\mathrm{re}}(\infty)\rvert m^{\frac{3}{4}}$	0.4375	1.207	0.0985
		$m = 10000$	$m = 40000$
R_1		0.750136	0.752129
R_2		0.756275	0.754295
$(R_2 - R_1)m^{\frac{3}{4}}$		6.139	6.126
ω_1^{im}		0.457920	0.458339
ω_2^{im}		0.456245	0.457502
$(\omega_1^{\mathrm{im}} - \omega_2^{\mathrm{im}})m^{\frac{1}{4}}$		0.1675	0.1674
$\tilde{\omega}_1^{\mathrm{re}}$		−0.3636139149	−0.3636139926 7
$\tilde{\omega}_2^{\mathrm{re}}$		−0.3636137489	−0.3636139718 2
$(\tilde{\omega}_1^{\mathrm{re}} - \tilde{\omega}_2^{\mathrm{re}})m^{\frac{3}{4}}$		0.1660	0.1668
$\lvert\omega_1^{\mathrm{im}} - \omega_1^{\mathrm{im}}(\infty)\rvert m^{\frac{1}{4}}$		0.0840	0.0841
$\lvert\tilde{\omega}_1^{\mathrm{re}} - \tilde{\omega}_1^{\mathrm{re}}(\infty)\rvert m^{\frac{3}{4}}$		0.0889	0.0889

TABLE 3. Asymptotic behaviour of the most-unstable inviscid modes for large m. Rows 1–3; spatial localization of the eigenfunction (R_1 and R_2 represent the locations of the two characteristic minima of the radial eigenfunction); rows 4–9: asymptotic closeness of the primary and secondary mode with increasing m; rows 10 and 11: approach of ω_1^{im} and $\tilde{\omega}_1^{\mathrm{re}}$ to their limiting values.

where the Reynolds number is based on the axial velocity excess of the steady flow and the radius of the viscous core, defined by the location of the maximum swirl velocity $V(r)$. The boundary conditions are the same as given for the inviscid problem. The first evidence of instabilities of a viscous nature for the trailing vortex were found recently by Khorrami, who solved the full equations using a staggered-grid method. The procedure used in this study is to first eliminate the pressure from the three momentum equations in the same fashion as for the inviscid analysis. This eliminates the need for a staggered grid, making the numerical solution of the problem straightforward. The reduced disturbance momentum equations are, assuming zero steady radial velocity:

$$\frac{\mathrm{i}}{Re}(\alpha u' + w'')^* + \left[\gamma - \frac{\mathrm{i}}{Re}\left(\frac{m^2+1}{r^2} + \alpha^2\right)\right](\alpha u + w') + (W'u)' + \frac{2\alpha}{r}\left(V - \frac{\mathrm{i}m}{rRe}\right)v + \left(\gamma' + \frac{2\mathrm{i}m^2}{r^3 Re}\right)w = 0, \quad (8a)$$

$$\frac{\mathrm{i}}{Re}\left[\alpha r(v')^* - m\left(w'' + \frac{w^*}{r}\right)\right] + \left[\gamma - \frac{\mathrm{i}}{Re}\left(\frac{m^2+1}{r^2} + \alpha^2\right)\right](\alpha r v - m w) + \left(V^* - \frac{2\mathrm{i}m}{r^2 Re}\right)\alpha r u - m W' u = 0, \quad (8b)$$

and along with the continuity equation (7a) constitute a sixth-order system for the disturbance velocities. Note however that (8a) is third order in the axial velocity, which means that an additional boundary condition is needed. Since we expect smoothly decaying solutions at large radius, one can simply set an additional derivative of w to zero at the outer boundary. The continuity equation can further be used to eliminate the axial velocity perturbation from these equations, leading to a seventh-order system of two equations, one of which is fourth-order in the radial velocity perturbation. However, as solution of the two-equation system generally requires a higher spectral resolution to achieve a similar accuracy, the advantage of having a smaller number of equations is lost.

Although the convergence of the eigenvalues is not as rapid with increasing resolution as that reported for the staggered method, this is likely due to the different coordinate stretchings used – Khorrami, Malik & Ash (1989) use a non-uniform coordinate transformation which spreads the outer-boundary points apart, allowing large values of R to be taken with relatively few basis functions. The algebraic stretching, on the other hand, does nothing special with the outer parts of the mesh, where the clustering of points due to the cosine spacing makes little physical sense. A comparison of the two methods, however, shows that while the former method allows good results to be obtained at lower computational costs when the Reynolds number is not too large (roughly within two orders of magnitude of the critical value), the algebraic stretching method has superior numerical properties at high Reynolds number, where the growth rate of the unstable viscous modes becomes quite small, requiring high spectral resolution for convergence. Additionally, the elimination of one equation in the present study reduces the order of the matrix eigenvalue problem for given N by 25%. Since the number of operations for the global eigenvalue method scales as $O(N^3)$, this reduces the work done (for the same number of basis functions per variable) by more than half. Finally, the fact that the presence of the viscous instabilities is confirmed using a different formulation effectively removes any doubts regarding their existence.

	Lessen & Paillet			Present study			
m	q_c	β_c	Re_c	q_c	β_c	Re_c	Re_c/m^2
1	−0.45	0.42	13.9	−0.337	0.415	13.905	—
2	−0.7	0.46	27.9	−0.466	0.475	26.26	6.565
3	−0.95	0.54	48.2	−0.515	0.479	46.91	5.2122
4	—	—	—	−0.535	0.476	73.11	4.5694
5	—	—	—	−0.545	0.473	105.29	4.2116
10	—	—	—	−0.557	0.464	356.32	3.5632
20	—	—	—	−0.558	0.460	1306.3	3.2658
50	—	—	—	−0.553	0.457	7682.8	3.0731
100	—	—	—	−0.550	0.456	2.9922×10^4	2.9922
1000	—	—	—	−0.544	0.456	2.8730×10^6	2.8730
10000	—	—	—	−0.542	0.456	2.8376×10^8	2.8376

TABLE 4. Viscous analysis of inviscid modes – critical parameters for the onset of instability

3.2. *Effects of finite Reynolds number on inviscid modes*

Lessen & Paillet (1974) were the first to study the effects of viscosity on the linearized stability of the trailing vortex. They found no modes that were viscous in nature, and found that the growth rates of the most-unstable inviscid modes rapidly approached their limiting values as the Reynolds number was increased. More recently, Khorrami *et al.* (1989) have raised questions about Lessen & Paillet's numerical technique, asserting that too small an outer-boundary radius ($R = 3$) was used in the integration of the governing equations. This, along with the fact that Lessen & Paillet did not find the maximum inviscid instability for this case correctly, makes their viscous results worth checking. Accurate results for $m = 1$ are particularly important since Lessen & Paillet report that this case has the lowest critical Reynolds number. Using the present numerical method, we find that $R = O(10)$ is sufficient to give six-figure accuracy for this case for most parameter values. The results for the most-unstable mode show that the location of the maximum disturbance growth rate in (q, α)-space shifts to smaller swirl and axial wavenumbers with decreasing Reynolds number. For $Re < 100$, the greatest instability shifts rapidly to lower α as viscosity stabilizes shorter-wavelength disturbances. All disturbances are damped below the critical Reynolds number of 13.905, the critical swirl and axial wavenumber being $q_c = -0.337$ and $\alpha_c = 0.415$. Somewhat surprisingly, Re_c and α_c are in good agreement with Lessen & Paillet's results, even though the critical value of swirl claimed by them differs substantially from the one found here.

For higher azimuthal wavenumbers, the same general behaviour is seen, the most-unstable modes shifting to longer-wave disturbances and more weakly swirling flow with decreasing Reynolds numbers. The critical parameter values for m ranging from 1 to 10000 are summarized in table 4, with the values found by Lessen & Paillet at low m given for comparison. The critical swirl and axial wavenumber asymptote to values of $q_c \approx -0.54$, $\beta_c = 0.456$ for large m, values somewhat different than those for the inviscid large-m disturbance modes. The results for larger m (the viscous computation of these modes again takes advantage of the localized nature of the eigenfunctions for $m \gg 1$, which occurs much as in the inviscid case) show that it is the ratio Re_c/m^2 which approaches a constant value as $m \to \infty$. The quadratic growth of Re_c with m is in agreement with an asymptotic prediction of Stewartson (1982),

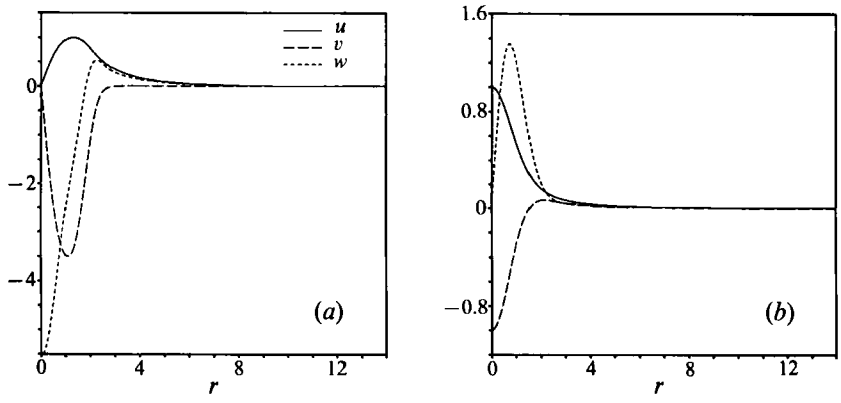

FIGURE 8. Velocity perturbation eigenfunctions for the (*a*) axisymmetric viscous mode ($m = 0$, $q = 1$, $\alpha = 0.5$, $Re = 10000$, $\omega = -0.016407\,1703 + \mathrm{i}\ 0.000\,184\,691$); (*b*) asymmetric viscous mode ($m = 1$, $q = 0.4$, $\alpha = 0.3$, $Re = 2000$, $\omega = 0.023\,455\,121\,3 + \mathrm{i}\ 0.000\,470\,698\,0$).

and the numerical calculation gives the constant of proportionality as slightly less than 3, as well as finding the asymptotic values of q_c and β_c. The viscous analysis thus demonstrates that although large-azimuthal-wavenumber modes are the most unstable in the strictly inviscid sense, they are also the most susceptible to the stabilizing action of viscosity. This means that the maximum instability of the flow at any finite Reynolds number (no matter how large) occurs at finite azimuthal wavenumber, which is physically more sensible than the inviscid result.

The results for low values of m of course do not address the perhaps more fundamental question of the validity of the steady flow profiles at low Reynolds numbers; it is likely that the velocities given in (1) are still qualitatively representative of the finite-Reynolds-number flow, but one would expect that a non-zero radial velocity $U(r, z)$, which for the trailing vortex scales as $o(Re^{-\frac{1}{2}})$ at large Reynolds numbers, might become important, and that the axial and azimuthal velocity distributions would be modified somewhat also. At low Re, the assumption of self-similarity used in deriving (1) also becomes questionable. In any case, the effects of low Reynolds numbers on the structure and stability of the basic flow are not completely clear, and the corresponding critical parameters should thus be taken more as a qualitative guide to the behaviour one might expect to see in flows having the same general character as the one studied here.

3.3. *Viscous instabilities*

The fact that the presence of viscosity can destabilize some flows, the most notable cases of this being boundary-layer and parallel shear flows, has been known for over half a century. The effects of viscosity on the stability of swirling flows, on the other hand, have been much less clear, with most analytical and numerical work having focused on the inviscid stability problem and the few numerical results in the viscous case supporting the (until recently) generally held contention that viscosity acts purely as a stabilizing agent for swirling flows. The first direct evidence of linearly destabilizing perturbations of a viscous nature were reported by Khorrami (1991), who found both an axisymmetric and a non-axisymmetric ($m = 1$) instability mode for the trailing vortex, both with growth rates several orders of magnitude smaller than those of highly unstable inviscid modes.

An important feature of these viscous instabilities is that both occur in regions of

Re	q^*	α^*	ω^{im}	$q_{unstable}$	$\alpha_{unstable}$
322.35	1.08	0.468	-4.96×10^{-7}	—	—
322.45	1.08	0.468	2.55×10^{-7}	—	—
350	1.08	0.471	1.82×10^{-4}	$1.01 < q < 1.15$	$0.33 < \alpha < 0.63$
400	1.08	0.472	4.27×10^{-4}	$0.97 < q < 1.18$	$0.26 < \alpha < 0.73$
600	1.07	0.464	8.30×10^{-4}	$0.89 < q < 1.23$	$0.15 < \alpha < 0.91$
10^3	1.05	0.444	9.03×10^{-4}	$0.83 < q < 1.26$	$0.08 < \alpha < 1.06$
10^4	0.929	0.280	2.23×10^{-4}	$0.54 < q < 1.29$	$0 < \alpha < 1.29$
10^5	0.82	0.22	2.73×10^{-5}	$0.28 < q < 1.30$	$0 < \alpha < 1.32$
10^6	0.40	0.18	3.07×10^{-6}	$0.12 < q < 1.30$	$0 < \alpha < 1.41$

TABLE 5. Location and growth rate corresponding to maximum instability, and range of unstable q and α, both *vs.* Reynolds number, for the axisymmetric viscous mode.

the q–α parameter space where no inviscid instability has been found. As noted by Khorrami, the outer-boundary radius R required for accurate calculation of viscous modes is somewhat larger than for the inviscid problem; we find R between 20 and 50 to be sufficient except at very low Reynolds numbers or for very long-wave disturbances. Real parts of the eigenfunctions for these two viscous instabilities at typical unstable parameter values are plotted in figure 8(a, b), with the maximum amplitude of the radial velocity perturbation normalized to unity. (In case a comparison of the eigenvalues corresponding to these eigenmodes with Khorrami's results is desired, it should be noted that he takes $W_\infty = 1$, which adds a factor α to the real wave speed in his results.)

3.4. *The axisymmetric viscous mode*

Because the disturbances are axisymmetric, the sense of rotation of the basic flow does not affect its stability; thus only positive swirl need be considered in this case. Data regarding the location and growth rate of maximum instability, along with the range of unstable q and α, are summarized for various Reynolds numbers in table 5. The flow initially becomes unstable at a Reynolds number of 322.42, with the unstable region growing rapidly in extent with increasing Reynolds numbers above the critical value. The location of maximum disturbance growth rate moves very little initially, but begins moving to lower swirls and axial wavenumbers fairly rapidly for Reynolds numbers of 10^3 and greater. Contours of constant disturbance growth rate for $Re = 1000$ and 10000 are plotted in figures 9(a) and 9(b), with the outermost contour representing the neutral curve. For $Re = 1000$, the flow is unstable for swirl in the range $0.83 < q < 1.26$ and axial wavenumbers $0.08 < \alpha < 1.06$. The area of the unstable region for $Re = 10000$ is more than double that at the lower Reynolds number, but the maximum growth rate, which begins to decrease for $Re \lesssim 900$, is only a quarter as great. For $Re = 10000$, the flow is unstable for swirls in the range $0.54 < q < 1.29$. The unstable region now just touches the zero-wavenumber axis, with unstable axial wavenumbers extending to a short-wave limit of roughly 1.29. The phase speeds of unstable disturbances for the latter case range from roughly -0.14 at the largest unstable swirl values to zero for the smallest. The negative phase speed shows that $\gamma(r)$ is of one sign, indicating the absence of a critical layer for these disturbance modes.

For large Reynolds numbers, the unstable region no longer expands to higher swirl, the large-q parts of the neutral curves for $Re = 10^4$, 10^5 and 10^6 being virtually indistinguishable. The unstable region does, however, continue to expand to lower

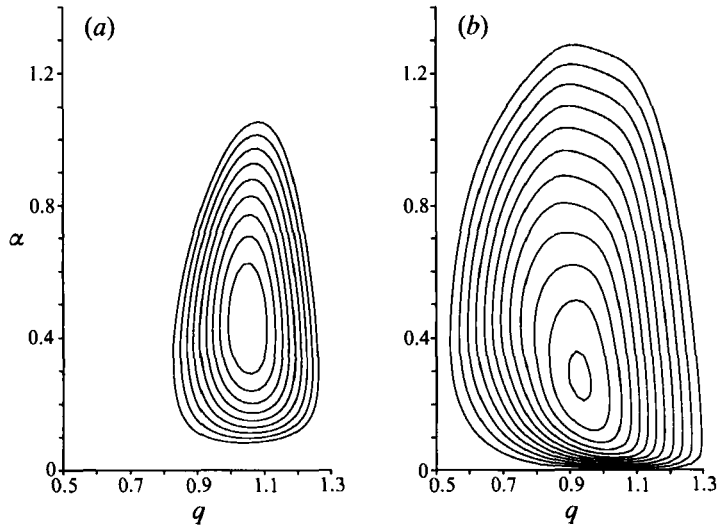

FIGURE 9. Contours of constant disturbance growth rate for the axisymmetric viscous mode at (*a*) $Re = 1000$ (10^{-4} per contour), (*b*) $Re = 10000$ (2×10^{-5} per contour).

Re	ω
10^3	$-0.017417059 + i8.140964 \times 10^{-4}$
10^4	$-0.016407170 + i1.846908 \times 10^{-4}$
10^5	$-0.016382486 + i1.883375 \times 10^{-5}$
10^6	$-0.016382232 + i1.883758 \times 10^{-6}$
10^7	$-0.016382230 + i1.883763 \times 10^{-7}$

TABLE 6. Axisymmetric mode eigenvalue *vs.* Reynolds number at fixed parameter values ($q = 1.0$, $\alpha = 0.5$).

values of swirl, the minimum q for instability for these three Reynolds numbers being 0.54, 0.28 and 0.12, respectively. At a given value of q, the range of unstable wavenumbers appears to approach a limit with increasing Re. For $q = 0.6$, for instance, the shortest unstable waves for any Reynolds number have $\alpha \approx 1.32$. It is not clear at what parameter values the shortest unstable wavelengths occur, as the range of unstable α at low swirl is still expanding for $Re = 10^6$. It appears that once a point comes to lie in the unstable region, it remains there with increasing Reynolds number, at least for the range of Re investigated here. The real part of the unstable eigenvalue at given q and α approaches a constant with increasing Reynolds number, but the growth rate decreases as $1/Re$, behaviour which is summarized in table 6. All figures given in the table are significant. Neutral stability curves for this mode at various Reynolds numbers ranging from 350 to 10^6 are plotted in figure 10.

Whether the unstable region comes to intersect the zero-swirl axis in a finite interval of axial wavenumbers at large Re or merely approaches it asymptotically is still an open question, but the Reynolds numbers in question are clearly very large. No secondary mode of instability was found for $Re \leqslant 10^7$ for the axisymmetric case, the only other converged modes found being strictly stable. While this does not rule out the possible existence of higher modes at larger Re, it makes it less likely that such modes would occur in actual aircraft wakes, which do not generally have Reynolds numbers based on core diameter greater than $O(10^7)$.

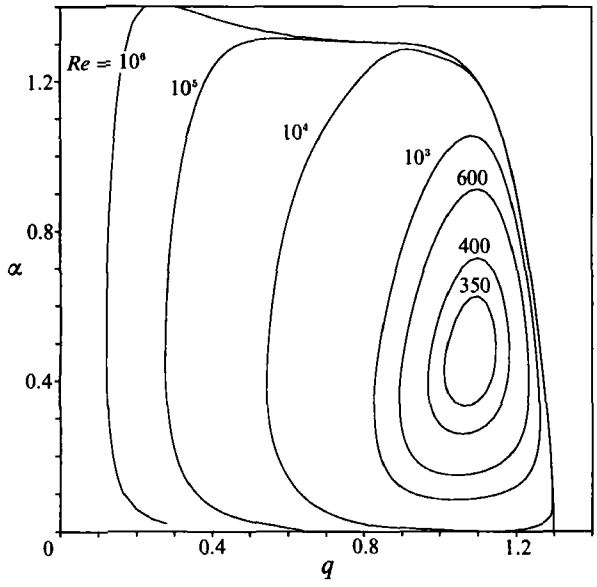

FIGURE 10. Neutral curves at various Reynolds numbers for the axisymmetric viscous mode.

Re	q^*	α^*	ω^{im}	q_{unstable}	$\alpha_{\mathrm{unstable}}$
17.5	0.475	0.336	-3.07×10^{-5}	—	—
17.6	0.477	0.338	8.17×10^{-5}	—	—
20	0.510	0.369	2.55×10^{-3}	$0.26<q<0.70$	$0.14<\alpha<0.55$
25	0.535	0.404	6.25×10^{-3}	$0.15<q<0.85$	$0<\alpha<0.70$
40	0.537	0.436	1.06×10^{-2}	$0.02<q<0.96$	$0<\alpha<0.91$
100	0.475	0.418	9.61×10^{-3}	$0<q<1.08$	$0<\alpha<1.13$
1000	0.24	0.21	1.66×10^{-3}	$0<q<1.08$	$0<\alpha<1.14$

TABLE 7. Location and growth rate corresponding to maximum instability *vs.* Reynolds number for the asymmetric viscous mode

3.5. *The asymmetric viscous mode*

An asymmetric viscous mode of instability, first reported by Khorrami, occurs for an azimuthal wavenumber, $m = 1$, for which inviscid modes which persist to quite low Reynolds numbers are also seen. This viscous instability, however, exists for positive swirl values beyond which any inviscid mode is stabilized. Also, the character of the unstable region for this mode is rather different than that of its axisymmetric counterpart. The flow first becomes unstable with respect to these asymmetric perturbations at a swirl of $q_c = 0.475$ and an axial wavenumber $\alpha_c = 0.336$. The critical Reynolds number for this mode of $Re_c = 17.527$ is much lower than for the axisymmetric mode (and quite close to that of the $m = 1$ inviscid mode). The maximum growth rates at $Re = O(10^2)$ are an order of magnitude greater than those of the axisymmetric mode, but begin to decay at much lower Reynolds numbers, so that at large Re the axisymmetric mode would appear to be the dominant form of instability, at least as far as small disturbances are concerned.

The location and value of the maximum growth rate for this mode are summarized in table 7 for various Reynolds numbers, as is the rough extent of the unstable region in the parameter space. The unstable region expands very rapidly for $Re > Re_c$,

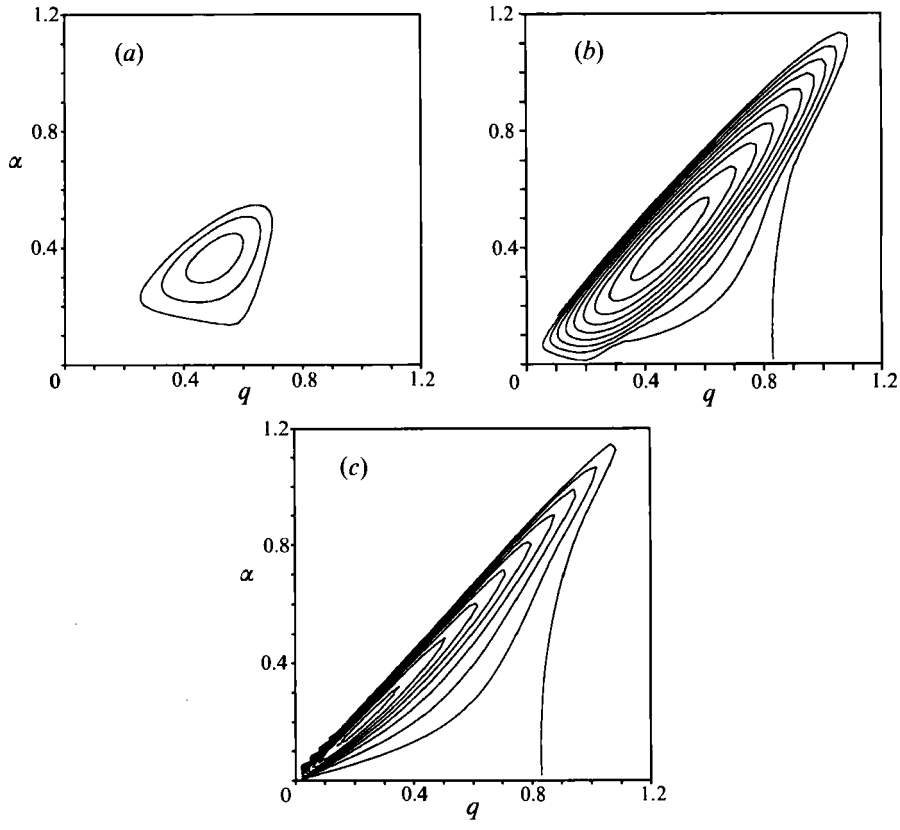

FIGURE 11. Contours of constant disturbance growth rate for the asymmetric viscous mode at (*a*) $Re = 20$ (10^{-3} per contour), (*b*) $Re = 100$ (10^{-3} per contour), (*c*) $Re = 1000$ (2×10^{-4} per contour).

moving rapidly toward the long-wave axis at Reynolds numbers slightly above the critical value. The unstable region has a maximum extent at a Reynolds number of roughly 100, its upper part beginning to narrow for larger Re. The interval of unstable swirl values reaches a limit of $q_{\text{unstable}} \in [0, 1.08]$, the upper limit being reached for wavenumbers which are near unity, the largest unstable swirl for long waves having a lower value, $q \approx 0.83$.

Contours of constant disturbance growth rate for Reynolds numbers of 20, 100 and 1000 are plotted in figure 11(*a–c*). At $Re = 20$, the unstable region has not yet reached the abscissa, but at Reynolds numbers which are only slightly higher, the lower right portion of the unstable region spreads rapidly toward lower α. For both higher-Reynolds-number cases the upper branch of the neutral curve proceeds roughly along the line given by $\alpha = 1.1q$. The maximum instability at given swirl is located very close to the upper branch, the growth rate decreasing very rapidly with α increasing from this point. On the other, long-wave side of the ridge formed by the maximum instability, the growth rates quickly drop roughly an order of magnitude, but then decay much more slowly as the lower branch of the neutral curve is approached. The phase speeds of unstable disturbance waves range from about -0.03 to 0.12, the positive values belonging to the shortest-wave disturbances at given q. As with the axisymmetric mode, the growth rates of this asymmetric mode decay at large Reynolds numbers, beginning to do so, however, at much lower Reynolds numbers. The unstable eigenvalue at fixed q and α but with Reynolds

Re	ω
10^2	$0.017279940 + i8.996067 \times 10^{-3}$
10^3	$0.023462141 + i9.790436 \times 10^{-4}$
10^4	$0.023453266 + i9.192278 \times 10^{-5}$
10^5	$0.023453788 + i8.6485 \times 10^{-6}$

TABLE 8. Asymmetric primary mode eigenvalue *vs.* Re at fixed parameter values ($q = 0.4$, $\alpha = 0.3$).

N	R	ω_1	ω_2
50	100	$0.000826463\,8 + i0.003\,914\,782\,39$	$0.000\,141\,769\,553 - i0.000\,168\,932\,9$
75	110	$-0.002\,005\,432\,8 + i0.000\,986\,162\,47$	$-0.000\,032\,656\,303 + i0.000\,232\,655\,1$
100	120	$-0.002\,234\,128\,3 + i0.000\,988\,908\,15$	$0.000\,035\,903\,501 + i0.000\,265\,609\,6$
150	140	$-0.002\,238\,716\,5 + i0.000\,988\,516\,41$	$0.000\,037\,017\,512 + i0.000\,266\,179\,4$
200	160	$-0.002\,238\,703\,6 + i0.000\,988\,516\,50$	$0.000\,037\,010\,727 + i0.000\,266\,188\,1$
250	180	$-0.002\,238\,703\,8 + i0.000\,988\,516\,55$	$0.000\,037\,010\,246 + i0.000\,266\,189\,2$
300	200	$-0.002\,238\,703\,9 + i0.000\,988\,516\,43$	$0.000\,037\,010\,243 + i0.000\,266\,189\,7$

TABLE 9. Convergence of primary and secondary asymmetric mode eigenvalues at $q = 0.5$, $\alpha = 0.05$, $Re = 25$

numbers varying over four orders of magnitude is tabulated in table 8. The real part of the eigenvalue again approaches a limit with increasing Re, but the growth rate decays somewhat more slowly than $1/Re$. This is likely due in part to the fact that the Reynolds numbers in question are not as large as those studied in the axisymmetric case, 10^5 being the upper limit at which accurate computations were still feasible.

Khorrami has described both this and the axisymmetric mode as long-wave instabilities, but this characterization should perhaps be refined. The maximum growth rates at all Reynolds numbers studied here occur at wavelengths which are the same order of magnitude as the radial extent of the viscous core of the vortex. No instability was found for wavelengths much shorter than this, but unstable long waves exist for both modes of instability, starting at Reynolds numbers less than an order of magnitude larger than the critical values.

In addition to the instability just described, we have found a family of unstable viscous modes for $m = 1$ which have not been reported previously. These modes are truly long wave in character, in that their unstable regions lie very close to the $\alpha = 0$ axis for all Reynolds numbers where instability is found. A convergence history of the primary- and secondary-mode eigenvalues is given in table 9. The critical Reynolds number for the secondary mode of roughly 20 is only slightly larger than that of the primary mode, but the behaviour of the instability with increasing Reynolds number is unusual. At $Re = 25$, the unstable region extends for the swirl range $0.4 < q < 1.15$ and to a short-wave limit of $\alpha = 0.134$. At $Re = 40$, the unstable region is much smaller, having roughly the same range of unstable α but with a range of unstable swirl of only $0.22 < q < 0.73$.

The tertiary and higher modes behave much like the secondary mode, except that they are unstable for a progressively smaller range of α and each has a maximum growth rate which is generally an order of magnitude or more smaller than that of the previous one. Plots of the variation with α of the real and complex parts of the eigenvalue corresponding to the primary and secondary mode at parameter values of $q = 0.4$, $Re = 40$ are plotted in figure 12 (the tertiary mode, which is unstable for

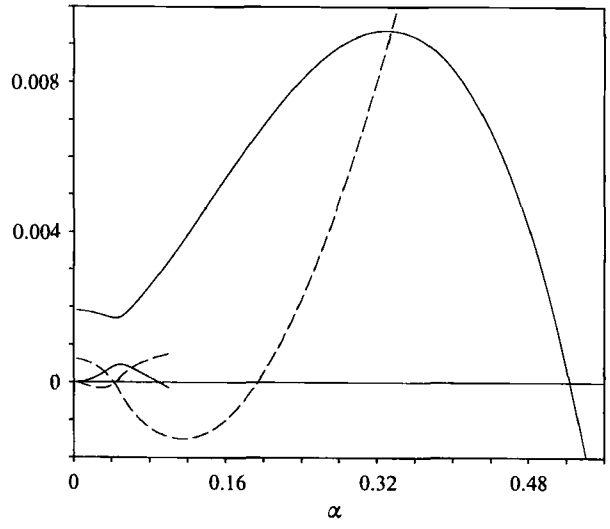

FIGURE 12. Real (dashed) and imaginary (solid) part of the $m = 1$ primary and secondary mode eigenvalues *vs.* α at $q = 0.4$, $Re = 40$.

$\alpha < 0.01$ and has a maximum growth rate of roughly 2×10^{-5}, is not visible at this scale). The physical import of these modes, however, should be viewed in the light of the fact that the parallel-flow assumption breaks down at small α, so a rigorous analysis of these very long-wave modes would need to take effects of non-parallelism of the basic flow into account. The primary mode, however, being the only one which persists to large Reynolds numbers, is of greatest interest, since swirling wakes which persist for long periods of time will tend to have low levels of viscosity.

4. Conclusions

In addition to yielding the first global pictures of inviscid instabilities of the trailing vortex, the results of this study provide the first direct numerical validation of the large-azimuthal-wavenumber asymptotic analysis of Leibovich & Stewartson. It has been shown that by taking advantage of the increasingly localized structure of the disturbance eigenfunctions for large m, accurate results are obtained up to azimuthal wavenumbers of 10000 and greater, and the agreement with the asymptotic theory is excellent. Not only the most unstable mode, but all of the unstable modes which are numerically well-resolved appear to possess growth rates which approach a finite value at large m, with the difference between the limiting eigenvalue and the eigenvalues at finite m vanishing as $m^{-\frac{1}{2}}$, and the multiple unstable modes coinciding to $O(m^{-\frac{1}{2}})$ in this limit. The numerical analysis is accurate enough to actually give the exact powers of m of the asymptotics; while an asymptotic description has already been established for the current problem, a versatile, high-quality numerical approach such as described could be a useful guide for the asymptotic theory in future problems of interest.

A viscous analysis of these fundamentally inviscid modes confirms the fact that the $m = 1$ case has the lowest critical Reynolds number, and the value found of $Re_c = 13.905$ is in good agreement with that claimed by Lessen *et al.*, although there are some discrepancies in the other critical parameters, particularly in the critical swirl, for the cases where comparisons are possible. In this study, critical parameters were found for azimuthal wavenumbers up to $m = 10000$, revealing that Re_c

increases roughly as $O(m^2)$ for $m \gg 1$, and that the critical values of swirl and scaled axial wavenumber approach limiting values as $m \to \infty$. The behaviour of the critical Reynolds number is important, since, although the large-m modes are the most unstable in the strictly inviscid sense, they are also shown to be the most susceptible to viscous stabilization.

Additionally, the viscous instabilities recently discovered by Khorrami (1991) have been mapped out in detail, and their behaviour as a function of viscosity is investigated, especially in the high-Reynolds-number limit. The critical Reynolds number for the axisymmetric mode was found to be 322.42, which is very close to that found by Khorrami. The asymmetric mode was found to possess a much lower critical Reynolds number of 17.527. For both modes, the extent of the unstable region (in swirl–axial wavenumber space) increases rapidly for Reynolds numbers increasing beyond their critical values. The unstable regions extend to infinitely long waves for Reynolds numbers roughly an order of magnitude larger than critical and appear to reach a maximum extent for $Re \gg Re_c$, the asymmetric mode doing so more quickly than the axisymmetric mode, which continues to extend to smaller and smaller swirl values even though the range of unstable wavenumbers for larger swirls has reached its maximum. For the $m = 1$ case, an additional family of long-wave instabilities has been shown to exist.

All computations for this study were performed on RISC-based workstations, using 64-bit precision real and 128-bit complex arithmetic. Information regarding any of the numerical procedures used will be provided on request. Funding for this work was provided by a NASA Graduate Student Researcher fellowship, NASA-G-NGT-50545, through Lewis Research Center.

REFERENCES

Barston, F. M. 1980 A circle theorem for inviscid steady flows. *Intl J. Engng Sci.* **18**, 477–489.

Batchelor, G. K. 1964 Axial flow in trailing line vortices. *J. Fluid Mech.* **20**, 645–658.

Batchelor, G. K. & Gill, A. E. 1962 Analysis of the stability of axisymmetric jets. *J. Fluid Mech.* **14**, 529–551.

Boyd, J. P. 1989 *Chebyshev and Fourier Spectral Methods.* Springer.

Duck, P. W. & Foster, M. R. 1980 The inviscid stability of a trailing line vortex. *Z. Angew. Math. Phys.* **31**, 524–532.

Duck, P. W. 1986 The inviscid stability of swirling flows: large wavenumber disturbances. *Z. Angew. Math. Phys.* **37**, 340–360.

Gary, J. & Helgason, R. 1970 A matrix method for ordinary differential eigenvalue problems. *J. Comput. Phys.* **5**, 169–187.

Golub, G. & VanLoan, C. 1989 *Matrix Computations*, 2nd edn. The Johns Hopkins University Press.

Gottlieb, D. & Orszag, S. A. 1977 *Numerical Analysis of Spectral Methods: Theory and Applications.* Philadelphia: Soc. Indus. & Appl. Maths.

Howard, L. N. & Gupta, A. A. 1962 On the hydrodynamic and hydromagnetic stability of swirling flows. *J. Fluid Mech.* **14**, 463–476.

Khorrami, M. R. 1991 On the viscous modes of instability of a trailing line vortex. *J. Fluid Mech.* **255**, 197–212.

Khorrami, M. R., Malik, M. R. & Ash, R. L. 1989 Application of spectral collocation techniques to the stability of swirling flows. *J. Comput. Phys.* **81**, 206–229.

Lin, C. C. 1966 *The Theory of Hydrodynamic Stability.* Cambridge University Press.

Lessen, M. & Paillet, F. 1974 The stability of a trailing line vortex. Part 2. Viscous theory. *J. Fluid Mech.* **65**, 769–779.

LESSEN, M., SINGH, P. J. & PAILLET, F. 1974 The stability of a trailing line vortex. Part 1. Inviscid theory. *J. Fluid Mech.* **63**, 753–763.

LEIBOVICH, S. & STEWARTSON, K. 1983 A sufficient condition for the instability of columnar vortices. *J. Fluid Mech.* **126**, 335–356.

STEWARTSON, K. 1982 The stability of swirling flows at large Reynolds number when subjected to disturbances with large azimuthal wavenumber. *Phys. Fluids* **25**, 1953–1957.

STEWARTSON, K. & CAPELL, K. 1985 On the stability of ring modes in a trailing line vortex: the upper neutral points. *J. Fluid Mech.* **156**, 369–386.

STEWARTSON, K. & LEIBOVICH, S. 1987 On the stability of a columnar vortex to disturbances with large azimuthal wavenumber: the lower neutral points. *J. Fluid Mech.* **178**, 549–566.

WILKINSON, J. H. 1965 *The Algebraic Eigenvalue Problem*. Oxford University Press.